Liquid Phase Stability Under an Extreme Temperature Gradient

Zhi Liang,[1] Kiran Sasikumar,[2] and Pawel Keblinski[1,2,*]

[1]Rensselaer Nanotechnology Center, Rensselaer Polytechnic Institute, Troy, New York 12180, USA
[2]Department of Materials Science and Engineering, Rensselaer Polytechnic Institute, Troy, New York 12180, USA

(Received 19 May 2013; published 25 November 2013)

Using nonequilibrium molecular dynamics simulations, we subject bulk liquid to a very high-temperature gradient and observe a stable liquid phase with a local temperature well above the boiling point. Also, under this high-temperature gradient, the vapor phase exhibits condensation into a liquid at a temperature higher than the saturation temperature, indicating that the observed liquid stability is not caused by nucleation barrier kinetics. We show that, assuming local thermal equilibrium, the phase change can be understood from the thermodynamic analysis. The observed elevation of the boiling point is associated with the interplay between the "bulk" driving force for the phase change and surface tension of the liquid-vapor interface that suppresses the transformation. This phenomenon is analogous to that observed for liquids in confined geometries. In our study, however, a low-temperature liquid, rather than a solid, confines the high-temperature liquid.

DOI: 10.1103/PhysRevLett.111.225701 PACS numbers: 64.70.fm, 68.03.Cd, 68.03.Fg

It is well known that a liquid confined in nanopores shows altered phase behavior compared to that of the bulk fluid [1]. For example, in a hydrophilic nanopore, it is found that a vapor can condense into a liquid at a temperature higher than the saturation temperature [2]. Both experimental and theoretical studies reveal that the shift of phase coexistence curves in confined fluids arises from the presence of wall-liquid interfaces and the associated surface tension [3–9].

Using molecular dynamics (MD) simulations, we show that an undersaturated vapor can condense into a liquid under a high-temperature gradient condition. Condensation of an undersaturated vapor is driven by the disappearance of the liquid-vapor interfaces, which reduces the free energy of the system. The observed phenomena require a very high-temperature gradient. Such high gradients are achievable in experiments of high-power laser heating of nanoparticles immersed in liquids [10,11].

Our model system is a bulk Ar fluid at 20 atm. We employ a truncated and shifted Lennard-Jones (LJ) 12-6 potential, with parameters $\sigma = 3.41$ Å and $\varepsilon = 10.3$ meV, for Ar-Ar interactions [12]. The cutoff distance is 3.2σ. The long-range corrections of the pressure and potential energy are not considered, as they cannot be applied consistently when multiple phases with widely different densities coexist in the same simulation cell. In all MD simulations, we use a velocity Verlet algorithm with a time step size of 8 fs for the integration of equations of motions [13]. We use the algorithm of Berendsen *et al.* [14] with time constants $\tau_T = 0.1$ ps and $\tau_P = 500$ ps to equilibrate the system to a preset temperature T and pressure P. At each preset temperature, the system is first equilibrated for 2 ns.

First, to establish the reference boiling point T_b of the bulk liquid, we study the coexistence of the liquid and vapor phase, both present in the same simulation cell with a planar liquid-vapor interface between them. In particular, we place a liquid slab of 2160 Ar atoms in the middle of a simulation box which has a length of $L_x = 19.2$ nm and cross section area A of $L_y = 3.84$ nm by $L_z = 3.84$ nm. Relatively large L_y and L_z are chosen to eliminate system size effects [15]. The box size is fixed during the simulation. Periodic boundary conditions (PBCs) are applied in all three directions. We equilibrate structures at multiple temperatures varying from 114 to 134 K. We use 14 ns for data collection and averaging at each temperature. By fitting the saturation pressure as a function of temperature, we determine T_b to be 124.33 ± 0.05 K at 20 atm (see the Supplemental Material for details [16]).

The second key parameter is the liquid-vapor surface tension, γ_{lv}. To determine its value, we equilibrate the liquid-vapor coexisting phases at $T = T_b$. Then, we monitor the value of the pressure tensor in 200 planar bins into which we divided the simulation cell. We then obtain the surface tension using the mechanical definition according to Irving and Kirkwood [17,18]

$$\gamma_{lv} = \frac{1}{2}\int_0^{L_x}[P_N(x) - P_T(x)]dx, \tag{1}$$

where P_N is the pressure normal to the interface and P_T is tangential pressure. The saturation pressure is the average value of P_N (see the Supplemental Material for details [16]). The factor of $1/2$ is used because two liquid-vapor interfaces are present in the simulation cell. Using the above described procedure at $T_b = 124.33$ K, we determined $\gamma_{lv} = 2.813 \pm 0.034$ mJ/m^2. These results are consistent with the experimental data $T_b = 130.01$ K and $\gamma_{lv} = 2.994$ mJ/m^2 at 20 atm [19]. Moderate differences between the experimental and modeling values can be

attributed to the neglect of the long-range pressure correction in MD simulations.

Finally, as required for thermodynamic analysis, we determined the Gibbs free energy difference between the bulk liquid phase and the vapor phase of Ar as a function of temperature. To do this, we evaluated the enthalpy H of bulk liquid and gas phases at temperatures varying from 124 to 136 K at $P = 20$ atm. The model system consists of 864 Ar atoms in a cubic box with PBCs to eliminate the size effect on thermodynamic properties of fluid [20]. Because of the nucleation barrier, vaporization of bulk liquid occurs at a temperature (136 K) much higher than T_b, while condensation of bulk vapor occurs at a temperature (113 K) much lower than T_b (see the Supplemental Material for details [16]). At each temperature, 15 ns are used for data collection and averaging. At $T = T_b = 124.33$ K, we obtained $\Delta H_b = 4138.9 \pm 1.4$ J/mol. Using this value the entropy difference at the boiling temperature is given by $\Delta S_b = \Delta H_b/T_b = -33.29 \pm 0.01$ J/mol K. Then, the Gibbs free energy difference as a function of temperature is determined by

$$\Delta G_{vl} = \Delta H_{vl} - T\Delta S_{vl}, \tag{2}$$

where ΔH_{vl} and ΔS_{vl} are, respectively, the enthalpy difference and entropy difference, between the liquid and vapor phases. ΔS_{vl} at a given temperature T_0 is determined by

$$\Delta S_{vl} = \Delta S_b + \int_{T_b}^{T_0} \frac{C_{P,l} - C_{P,v}}{T}\, dT, \tag{3}$$

where $C_{p,l} = dH_l/dT$ and $C_{p,v} = dH_v/dT$ are the specific heat of Ar at the liquid and vapor phases, respectively.

Now, we turn our attention to MD simulations under a high-temperature gradient. As shown in Fig. 1, the bulk fluid contains 8640 Ar atoms. PBCs are applied in all three directions. The barostat is applied in the heat flux x direction. The cross section area of the simulation box is fixed at $L_y = 3.84$ nm by $L_z = 3.84$ nm in the simulation. In all cases, the liquid Ar at 20 atm are first equilibrated for 2 ns at 125 K. After the system reaches the preset temperature and pressure, the global thermostat is turned off, and nonequilibrium MD (NEMD) simulations are performed. The barostat is still applied to maintain the pressure at 20 atm (see the Supplemental Material [16] for pressure distribution in the fluid). To generate a temperature gradient in the bulk fluid, we set the region from $x = 0$ to $x = 3.84$ nm as the heat source, and the region from $x = L_x/2$ to $x = L_x/2 + 3.84$ nm as the heat sink (see Fig. 1). The heat source temperature T_h is gradually increased to 136 K, and the heat sink temperature T_l is fixed at 100 K to ensure that the Ar around the heat sink region is in the liquid state. T_h and T_l are maintained in the MD simulation by velocity rescaling at each time step [21]. For each T_h, 7 ns are used to allow the system to reach a steady state.

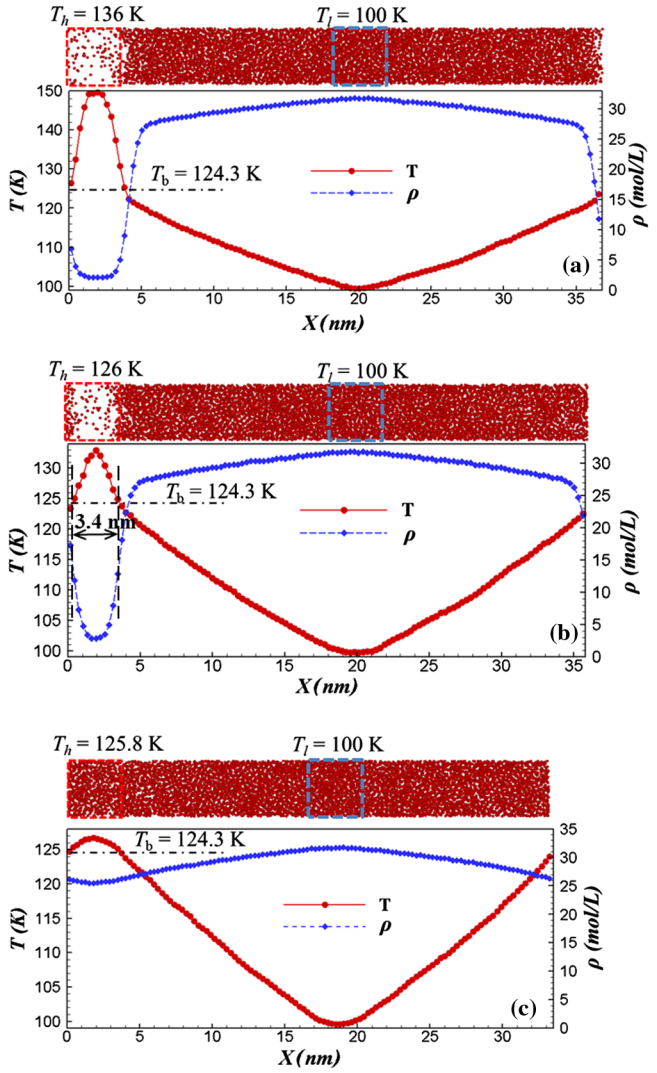

FIG. 1 (color online). Snapshot of fluid Ar and the corresponding temperature and density profiles for (a) $T_h = 136$ K and $T_l = 100$ K. (b) $T_h = 126$ K and $T_l = 100$ K. The separation between two interfaces is about 3.4 nm. The interface is defined at the plane where $T = T_b = 124.3$ K. (c) $T_h = 125.8$ K and $T_l = 100$ K. The uncertainties of temperature in the gas phase and the liquid phase are within 0.5 and 0.15 K, respectively.

We found that no vaporization occurs until T_h reaches ~136 K. For example for $T_h = 125.8$ K the hot liquid region is stable [see Fig. 1(c)] despite the fact that it is above the boiling point. One can argue that we simply do not observe vapor due to the kinetic barrier for the phase change. To address this argument, we increased T_h to 136 K to force vapor phase formation. The structure and the corresponding steady state temperature and density profiles are shown in Fig. 1(a). The temperature at the liquid-vapor interface is around $T_b = 124.3$ K, which is consistent with the thermodynamics boiling point. Subsequently, we use the above liquid-vapor structure at $T_h = 136$ K as the initial conditions for the quenching simulation. In the quenching simulation, T_l is fixed at

100 K and T_h is set to gradually lower temperatures. Through four independent runs, we observed the condensation of the undersaturated vapor occurs between $T_h = 126.0$ K and $T_h = 125.8$ K. A more precise determination of T_h at which condensation occurs is difficult since the uncertainty of temperature in our NEMD simulation is ± 0.1 K. The result demonstrates that under very high-temperature gradient, liquid can be locally above the boiling point and that this is not caused by the kinetic barrier for the phase change but has a more fundamental origin.

When vapor condensation occurs, the separation between two gas-liquid interfaces is about 3.4 nm as shown in Fig. 1(b). The interface is defined at the plane where $T = T_b = 124.3$ K. To investigate if the collapse of the gas phase is simply due to proximity of the two interfaces and possible attraction between them, we carried out equilibrium MD simulations at 125.8 K and 20 atm. Similar to the aforementioned simulation in the calculation of liquid-vapor surface tension we first performed a *NVT* simulation at 125.8 K. Then we adjusted the simulation box size L_x which leads to two liquid-vapor interfaces separating by ~ 3.0 nm. Subsequently, the barostat is applied in the x direction to maintain the system at 20 atm. Instead of condensation of the gas phase as we found in the NEMD simulation, in the equilibrium MD simulation liquid phase changes to the vapor phase (see the Supplemental Material [16] for details). Hence, we conclude that the condensation of undersaturated vapor in the presence of temperature gradients is not caused by interactions between liquid-gas interfaces.

To investigate why the gas-liquid phase transition occurs at a temperature between $T_h = 125.8$ K and $T_h = 126$ K, we resort to local free-energy based analysis. We will assume that despite the large temperature gradient liquid (or vapor) is at local thermal equilibrium. Therefore, at a given temperature characterizing a slab of material at position x, the free energy difference per unit length, $\Delta G_{vl}(x)$, is given by Eq. (2). The total ΔG_{vl} is determined by integrating $\Delta G_{vl}(x)$ over the vapor region. We define the vapor region as the region residing between liquid-vapor interfaces.

Using the equilibrium fluid properties, temperature, and density simulation data for $T_h = 126$ K shown in Fig. 1(b) and error propagation analyses [22], we obtained the total $\Delta G_{vl}/A$ of Ar in the vapor region equal to 6.35 ± 0.24 mJ/m^2. This can be compared with the change of the free energy due to the disappearance of the two liquid-vapor interfaces, which is $-2\gamma_{lv} = -5.62 \pm 0.07$ mJ/m^2. This is a quite striking numerical agreement, considering that in our analysis we assumed that the vapor (or liquid) is in a local thermal equilibrium despite the huge temperature gradient. Furthermore, this agreement suggests that one can determine the state of the system under high-temperature gradient from equilibrium criterion considerations.

Another possible way to do the thermodynamic analysis is to use the temperature and density profile of the liquid at $T_h = 125.8$ K. As shown in Fig. 1(c), there is a superheated liquid region where the temperature is higher than $T_b = 124.3$ K. The density of liquid in this region is essentially the same as that of bulk liquid at thermal equilibrium. Using the equilibrium fluid properties, we obtained 5.04 ± 0.33 mJ/m^2 as the total $\Delta G_{vl}/A$ of Ar in the superheated liquid region at $T_h = 125.8$ K, which is slightly smaller than $2\gamma_{lv} = 5.62$ mJ/m^2. This result indicates that the gas-liquid phase transition should occur at a temperature slightly higher than $T_h = 125.8$ K, which is consistent with the MD simulation result.

In the above MD simulation, the length of heat source region, L_h, is fixed at 3.84 nm. To investigate if the size of heat source region affects the simulation results, we reduced L_h to 2.56 nm and performed NEMD simulations. We found $T_h = 128.3 \pm 0.1$ K and the length of vapor region is ~ 2.9 nm when condensation occurs. In this case, the heat source region is shorter than the vapor region. Hence, the heat source region only contains high-temperature vapor phase. Consequently, the condensation occurs at $T_h = 128.3$ K (for $L_h = 2.56$ nm) which is higher than $T_h = 125.8$ K (for $L_h = 3.84$ nm). For $L_h = 2.56$ nm at $T_h = 128.3$ K, the total $\Delta G_{vl}/A$ of Ar in the vapor region equals to 6.11 ± 0.27 mJ/m^2, which is again close to $2\gamma_{lv} = 5.62 \pm 0.07$ mJ/m^2.

The results given above show that the increased condensation temperature arises from the nanoscale confinement of superheated liquid by a normal liquid due to the presence of a high-temperature gradient. However, it is rather difficult, if not impossible, to realize experimentally the local heating of a pure liquid, as used in our MD simulations. To connect our study with a more realistic situation, we also investigated how the temperature confinement affects the phase change of a fluid near a hot solid wall. To this extent, we carried out NEMD simulations on fluid Ar on a solid substrate. As shown in Fig. 2, the model system consists of a solid Kr in contact with fluid Ar. PBCs are applied in all three directions. The aforementioned Ar-Ar LJ potential describes all the interatomic interactions. The Kr atoms in the solid slab are initially arranged into a [1 0 0]-oriented perfect fcc crystal with 5 unit cells in each of the x, y, and z directions. In addition to the LJ potential, atoms in the solid slab are connected to their neighbors with FENE springs $V(r) = -0.5kR_0^2 \ln[1 - (r/R_0)^2]$, with $k = 30\varepsilon/\sigma^2$ and $R_0 = 1.5\sigma$ [23] to prevent the melting of the solid. With the LJ and FENE potentials, the lattice constant of the solid is about 4.6 Å. There are totally 4000 Ar atoms in the system. With these settings, we mimic a liquid on a wetting surface.

Similar to the MD simulation in the pure fluid Ar, the model system is first equilibrated to 20 atm and 100 K, and then NEMD simulations are carried out by setting the solid slab as the heat source and the center of the fluid slab as

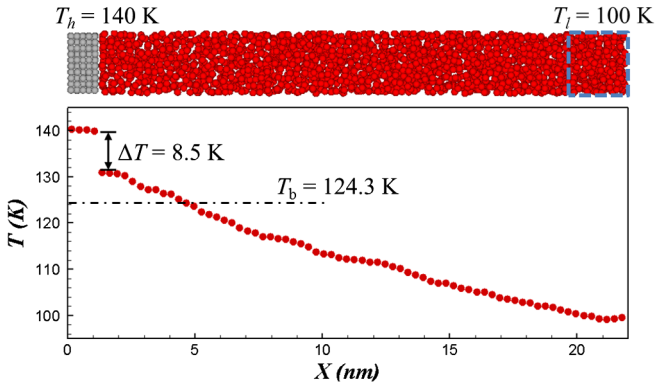

FIG. 2 (color online). Snapshot and temperature profile of the fluid near the hot solid surface at $T_h = 140$ K for $\varepsilon_{SF} = \varepsilon$. The model system has a symmetric structure. Only half of the simulation box is shown.

heat sink. In the NEMD simulation, T_l is fixed at 100 K, and T_h is gradually increased to 200 K to generate an Ar vapor near the solid surface. At the steady state, due to the high-temperature gradient, the solid slab and the liquid phase confine the vapor phase. Subsequently, we gradually decrease T_h and find that the condensation of undersaturated Ar occurs at $T_h = 140$ K. A snapshot of the solid-liquid system at $T_h = 140$ K and the corresponding temperature profile is shown in Fig. 2. Due to the interfacial thermal resistance, the maximum liquid temperature equals 130.8 K, which is much lower than the solid temperature, however, it is also much larger than the boiling temperature $T_b = 124.3$ K.

After the condensation, the solid-vapor and liquid-vapor interfaces disappear and a solid-liquid interface appears. Hence, the change of the free energy associated with the phase change is γ_{sl}—$(\gamma_{sv} + \gamma_{lv})$, where γ_{sl} and γ_{sv} are solid-liquid surface tension and solid-vapor surface tension, respectively. On a wetting surface, $\gamma_{sl} < \gamma_{sv}$, which indicates γ_{sl}—$(\gamma_{sv} + \gamma_{lv}) < -\gamma_{lv}$. This is consistent with the fact that the vapor condenses into liquid at a temperature higher than $T_b = 124.3$ K.

In the MD simulation, γ_{sl} and γ_{sv} can be tuned by setting the solid-fluid interaction strength ε_{SF} to different values. As ε_{SF} decreases, the contact angle (θ) of liquid on the solid surface increases. Using the Young's law [24], we obtain γ_{sl}—$(\gamma_{sv} + \gamma_{lv}) = -\gamma_{lv}(1 + \cos\theta)$. Hence, the maximum liquid temperature after condensation should decrease as ε_{SF} becomes smaller and θ becomes larger. We reduce ε_{SF} from ε to $\varepsilon/4$ and carry out the same NEMD simulation. It is found the maximum liquid temperature after condensation reduces from 130.8 K ($\varepsilon_{SF} = \varepsilon$) to 127.4 K ($\varepsilon_{SF} = \varepsilon/4$), which is consistent with the thermodynamic prediction.

In summary, we studied the phase behavior of fluid Ar under a high-temperature gradient condition using MD simulations. Because of the temperature gradient, the vapor phase is confined by the liquid phase in the fluid. The condensation of the undersaturated gas Ar accompanies the disappearance of liquid-vapor interfaces, which lead to a negative change in free energy. The condensation temperature obtained from the MD simulation is consistent with the thermodynamic prediction. The temperature confinement effect is also observed in liquid near a hot solid surface. The condensation temperature of undersaturated vapor near the solid surface is affected by the solid-fluid interaction strength.

This work is supported by NSF Grant No. CBET-1033354. We would like to thank Meng Shen for useful discussions on the thermodynamic analysis.

*keblip@rpi.edu

[1] L. D. Gelb, K. E. Bubbins, R. Radhakrishnan, and M. Sliwinska-Bartkowiak, Rep. Prog. Phys. **62**, 1573 (1999).
[2] K. Yasuoka, G. T. Gao, and X. C. Zeng, J. Chem. Phys. **112**, 4279 (2000).
[3] H. K. Christenson, Phys. Rev. Lett. **73**, 1821 (1994).
[4] K. Binder, D. P. Landau, and A. M. Ferrenberg, Phys. Rev. Lett. **74**, 298 (1995).
[5] S. M. Gatica, M. M. Calbi, and M. W. Cole, Phys. Rev. E **59**, 4484 (1999).
[6] F. Restagno, L. Bocquet, and T. Biben, Phys. Rev. Lett. **84**, 2433 (2000).
[7] K. T. Kholmurodov, K. Yasuoka, and X. C. Zeng, J. Chem. Phys. **114**, 9578 (2001).
[8] Y. Liu, Y. Men, and X. Zhang, J. Chem. Phys. **137**, 104701 (2012).
[9] T. Koishi, S. Yoo, K. Yasuoka, X. C. Zeng, T. Narumi, R. Susukita, A. Kawai, H. Furusawa, A. Suenaga, N. Okimoto, N. Futatsugi, and T. Ebisuzaki, Phys. Rev. Lett. **93**, 185701 (2004).
[10] M. Hu, P. Hristina, and G. V. Hartland, Chem. Phys. Lett. **391**, 220 (2004).
[11] A. Plech, V. Kotaidis, S. Grésillon, C. Dahmen, and G. von Plessen, Phys. Rev. B **70**, 195423 (2004).
[12] G. C. Maitland, M. Rigby, E. B. Smith, and W. A. Wakeham, *Intermolecular Forces: Their Origin and Determination* (Clarendon Press, Oxford, 1981).
[13] D. Frenkel and B. Smit, *Understanding Molecular Simulation* (Academic Press, San Diego, 2002), p. 75.
[14] H. J. C. Berendsen, J. P. M. Postma, W. F. Van Gunsteren, A. Di Nola, and J. R. Haak, J. Chem. Phys. **81**, 3684 (1984).
[15] A. Trokhymchuk and J. Alejandre, J. Chem. Phys. **111**, 8510 (1999).
[16] See Supplemental Material at http://link.aps.org/supplemental/10.1103/PhysRevLett.111.225701 for simulation details.
[17] J. P. R. B. Walton, D. J. Tildesley, J. S. Rowlinson, and J. R. Henderson, Mol. Phys. **48**, 1357 (1983).
[18] J. G. Kirkwood and F. P. Buff, J. Chem. Phys. **17**, 338 (1949).
[19] Thermophysical Properties of Fluid Systems in NIST Chemistry WebBook, NIST Standard Reference

Database Number 69, edited by E. W. Lemmon, M. O. McLinden, and D. G. Friend.

[20] S.-N. Lou, A. Strachan, and D. C. Swift, J. Chem. Phys. **120**, 11 640 (2004).

[21] P. Jund and R. Jullien, Phys. Rev. B **59**, 13 707 (1999).

[22] H. H. Ku, J. Res. Natl. Bur. Stand. Sec. C: Eng. Inst. **70C**, 263 (1966).

[23] S. Merabia, P. Keblinski, L. Joly, L. J. Lewis, and J. L. Barrat, Phys. Rev. E **79**, 021404 (2009).

[24] J. S. Rowlinson and B. Widom, *Molecular Theory of Capillarity* (Oxford University Press, Oxford, 1989).